Stability of the $q/3$ fractional quantum Hall states

Yang Liu, J. Shabani, and M. Shayegan
Department of Electrical Engineering, Princeton University, Princeton, New Jersey 08544, USA
(Received 16 April 2011; revised manuscript received 1 September 2011; published 3 November 2011)

Magnetotransport measurements in a wide GaAs quantum well in which we can tune the Fermi energy (E_F) to lie in different Landau levels of the two occupied electric subbands reveal a remarkable pattern for the appearance and disappearance of fractional quantum Hall states at $\nu = 10/3$, $11/3$, $13/3$, $14/3$, $16/3$, and $17/3$. The data provide direct evidence that the $q/3$ states are stable and strong even at such high fillings as long as E_F lies in a ground-state ($N = 0$) Landau level of either of the two electric subbands, regardless of whether that level belongs to the symmetric or the antisymmetric subband. Evidently, the node in the out-of-plane direction of the antisymmetric subband does not destabilize the $q/3$ fractional states. On the other hand, when E_F lies in an excited ($N > 0$) Landau level of either subband, the wave function node(s) in the in-plane direction weaken or completely destabilize the $q/3$ fractional quantum Hall states. Our data also reveal that the strength of the $q/3$ fractional states near the crossing of two Landau levels belonging to the two subbands depends on the relative spin polarization of the levels; specifically, the states remain stable very near the crossing if the two levels have parallel spins.

DOI: 10.1103/PhysRevB.84.195303 PACS number(s): 73.43.Fj, 73.21.Fg, 73.43.Nq, 73.43.Qt

I. INTRODUCTION

The fractional quantum Hall (FQH) effect,[1] signaled by the vanishing of the longitudinal resistance and the quantization of the Hall resistance, is the hallmark of an interacting two-dimensional electron system (2DES) in a large perpendicular magnetic field. It is a unique incompressible quantum liquid phase described by the celebrated Laughlin wave function.[2] In a standard, single-subband 2DES confined to a low-disorder GaAs quantum well, the FQH effect is most prominently observed at low Landau level (LL) filling factors $\nu < 2$, where the Fermi energy (E_F) lies in the spin-resolved LLs with the lowest orbital index ($N = 0$).[3] The strongest states are seen at the $q/3$ fractional fillings, namely at $\nu = 1/3$, $2/3$, $4/3$, and $5/3$. In contrast, as illustrated in Fig. 1(a), when E_F lies in the second ($N = 1$) set of LLs ($2 < \nu < 4$), the equivalent $q/3$ states at $\nu = 7/3$, $8/3$, $10/3$, and $11/3$ are much weaker.[4,5] In yet higher LLs ($\nu > 4$), for example, at $\nu = 13/3$, $14/3$, $16/3$, and $17/3$, which correspond to E_F being in the third ($N = 2$) set of LLs, the FQH states are essentially absent[6–8] [see Fig. 1(a)]. This absence is believed to be a result of the larger extent of the electron wave function (in the 2D plane) and its extra nodes that modify the (exchange-correlation) interaction effects and favor the stability of various nonuniform charge density states (e.g., stripe phases) over the FQH states.[9–13]

Recently, the FQH effect was examined in a wide GaAs quantum well where two electric subbands are occupied.[14] A main finding of Ref. 14 is highlighted in Fig. 1(b): When the Fermi level (E_F) lies in the $N = 0$ LLs of the antisymmetric electric subband, the even-denominator FQH states (at $\nu = 5/2$ and $7/2$) are absent and, instead, strong FQH states are observed at $q/3$ fillings $\nu = 7/3, 8/3, 10/3$, and $11/3$, as well as at $q/5$ fillings such as $12/5$, $13/5$, $17/5$, and $18/5$. Here we extend the measurements in this two-subband system and examine the stability of the $q/3$ FQH states at even higher fillings as we tune the position of E_F to lie in different LLs of the two subbands. At a fixed 2DES density we observe a remarkable pattern of alternating appearance and disappearance of the $q/3$ states as we tune the subband separation and the position of E_F. The data demonstrate that the $q/3$ states are stable even at filling factors as high as $\nu = 17/3$, as long as E_F lies in a ground state ($N = 0$) LL, regardless of whether that LL belongs to the symmetric or antisymmetric subband.

Our data also provide evidence that the stability of $q/3$ FQH states *near* the crossing (at E_F) of two LLs belonging to two subbands depends on the relative spin configuration of the two crossing LLs. More specifically, the $q/3$ FQH states seem to disappear suddenly when the two crossing LLs have *antiparallel* spins. But when the levels have *parallel* spins, the states remain stable near the crossing and disappear slowly. We provide self-consistent in-field calculations to examine a possible "pinning" of the crossing levels in a finite range of magnetic field. The pinning allows for a charge transfer between the crossing levels, and this charge transfer in turn helps bring the charge distribution at high fields close to the zero-field distribution. We use the results of such calculations to further discuss the stability of the $q/3$ FQH states near the LL crossings.

II. SAMPLE AND EXPERIMENTAL DETAILS

Our sample, grown by molecular beam epitaxy, is a 55-nm-wide GaAs quantum well (QW) bounded on each side by undoped $Al_{0.24}Ga_{0.76}As$ spacer layers and Si δ-doped layers.[15] We fitted the sample with an evaporated Ti/Au front gate and an In back gate to change the 2D electron density n and tune the charge distribution symmetry and the occupancy of the two electric subbands, as demonstrated in Fig. 2. This tunability, combined with the very high mobility ($\sim$400 m^2/V s) of the sample, is key to our success in probing the strength of the $q/3$ states at high fillings.

When the QW in our experiments is "balanced," that is, the charge distribution is symmetric, the occupied subbands are the symmetric (S) and antisymmetric (A) states [see the lower panels in Figs. 2(a) and 2(b)]. When the QW

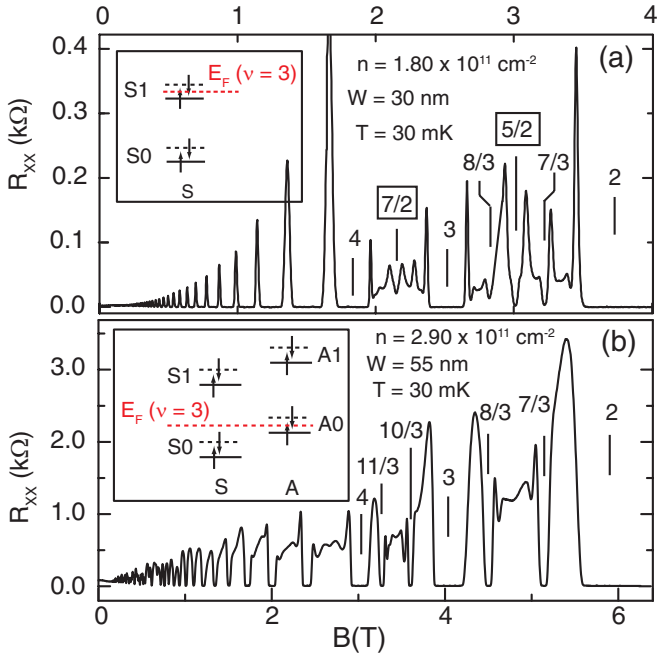

FIG. 1. (Color online) Longitudinal resistance (R_{xx}) vs magnetic field (B) for electrons confined to: (a) a narrow (well-width $W =$ 30 nm) and (b) a wide ($W = 55$ nm) GaAs quantum well. In (a) FQH states at $\nu = 5/2$ and $7/2$ can be clearly seen, but the states at $\nu = 7/3$ and $8/3$ are weak. In contrast, the even-denominator states are absent in (b) but strong FQH states are seen at $\nu = 7/3$, $8/3$, $10/3$, and $11/3$. The insets schematically show the positions of the spin-split LLs of the symmetric (S) and antisymmetric (A) subbands; the indices $N = 0$ and 1 indicate the lowest and the excited LLs, respectively. The subband separation for the trace in (b) is 24 K.

is "imbalanced," the two occupied subbands are no longer symmetric or antisymmetric; nevertheless, for brevity, we still refer to these as S (ground state) and A (excited state). In our experiments we carefully control the electron density and charge distribution symmetry in the QW by applying back- and front-gate biases.[16,17] For each pair of gate biases, we measure the occupied subband electron densities from the Fourier transforms of the low-field ($B \leqslant 0.5$ T) Shubnikov–de Haas oscillations. These Fourier transforms, examples of which are shown in Fig. 2(c), exhibit two peaks (B_S and B_A) whose frequencies, multiplied by $2e/h$, give the subband densities n_S and n_A. The difference between these densities directly gives the subband separation Δ through the expression $\Delta = \frac{\pi\hbar^2}{m^*}(n_S - n_A)$, where m^* is the electron effective mass. Note that, at a fixed total density, Δ is smallest when the charge distribution is balanced and it increases as the QW is imbalanced. Figure 2(d) shows the measured Δ as a function of the charge δn transferred between the back and front sides of the QW. Note that we measure δn from the change in the sample density induced by the application of either the back-gate or the front-gate bias.

III. MAGNETOTRANSPORT DATA

Figure 3 shows a series of longitudinal resistance (R_{xx}) vs magnetic field (B) traces taken at a fixed density $n = 2.12 \times 10^{11}$ cm^{-2} as the subband spacing is increased. The y axis is Δ, which is measured from the low-field Shubnikov–de Haas oscillations of each trace. The same data are interpolated and presented in a color-scale plot in Fig. 4(a). In Fig. 5 we show a color-scale plot of the data in the low field regime.

In Figs. 3, 4(a), and 5 we observe numerous LL coincidences at various integer filling factors, signaled by a weakening or disappearance of the R_{xx} minimum. For example, the R_{xx} minimum at $\nu = 4$ is strong and wide at all values of Δ except near $\Delta = 32$ and 58 K, marked by squares in Fig. 4(a), where it becomes narrow or disappears. Such coincidences can be easily explained in a simple, qualitative fan diagram of the LL energies in our system as a function of increasing Δ, as schematically shown in Fig. 4(b). In this figure we denote an energy level by its subband index (S or A), LL index ($N = 0,1,2,\ldots$), and spin ($\uparrow$ or $\downarrow$). Also indicated in Fig. 4(b) are the separations between various levels: the cyclotron energy ($E_C = \hbar eB/m^*$), Zeeman energy ($E_Z = g^*\mu_B B$, where g^* is the effective Landé g factor), and

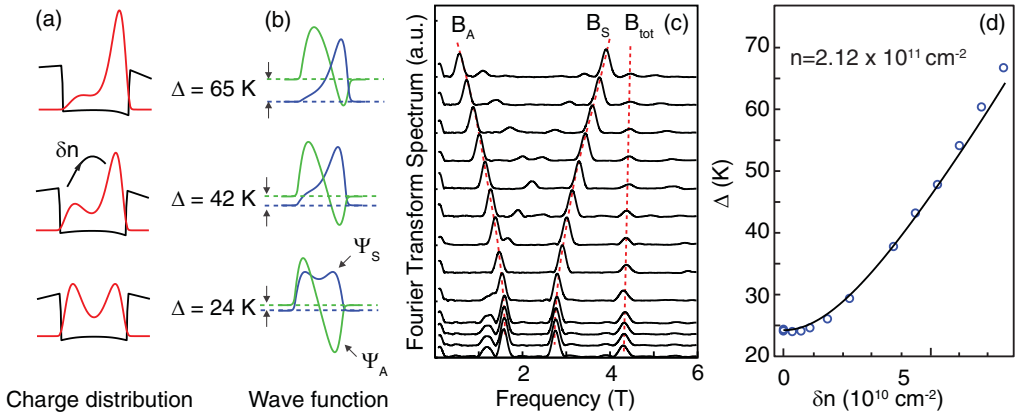

FIG. 2. (Color online) (a) Charge distribution (red) and potential (black), and (b) wave functions from self-consistent simulations for a 55-nm-wide GaAs QW. The charge density is kept fixed at $n = 2.12 \times 10^{11}$ cm^{-2}. The subband separation Δ is the smallest when the QW is balanced (bottom panels), and increases as the QW is imbalanced. (c) The Fourier transform spectra of the measured low-field Shubnikov–de Haas oscillations. Each spectrum exhibits two main peaks, denoted as B_A and B_S, whose separation increases as the QW is imbalanced (from bottom to top). (d) The subband separation Δ determined from the Fourier transforms through $\Delta = \frac{he}{m^*}(B_S - B_A)$, plotted as a function of the charge distribution asymmetry δn. The solid curve represents Δ vs δn from self-consistent calculations for a 55-nm-wide GaAs QW.

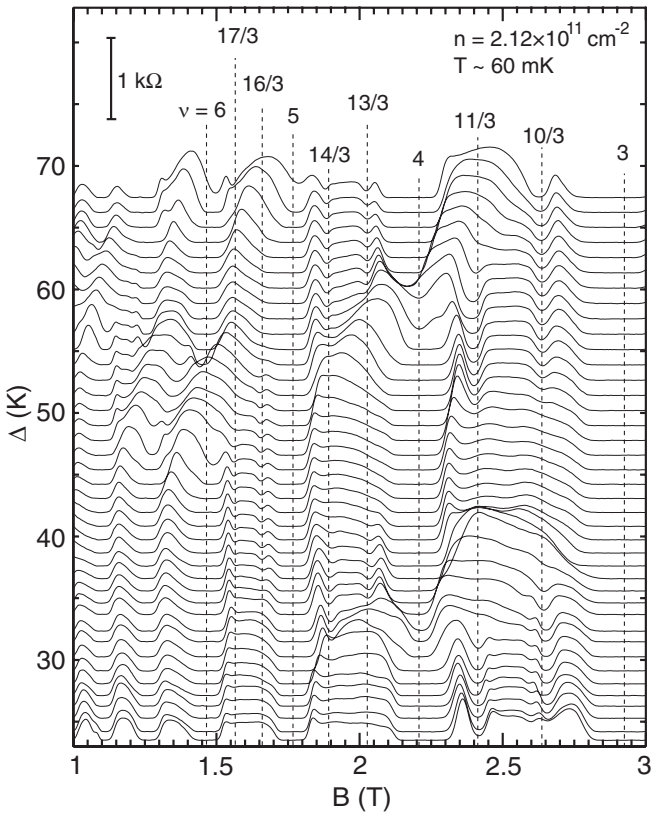

FIG. 3. Waterfall plot of R_{xx} vs B taken at a fixed density $n = 2.12 \times 10^{11}$ cm^{-2} as the subband separation (Δ) is increased. The scale for R_{xx} is indicted in the upper left (0 to 1 kΩ). Each trace is shifted vertically so that its zero (of R_{xx}) is aligned with its measured value of Δ which is used as the y axis of the waterfall plot. Vertical lines mark the field positions of the filling factors ν.

Δ. From Fig. 4(b) it is clear that the condition for observing a LL coincidence at odd fillings is $\Delta = iE_C$, while for coincidences at even fillings, the condition is $\Delta = iE_C \pm E_Z$; in both cases, i is a positive integer.

In Figs. 4(a) and 4(b), we have indicated the two coincidences at $\nu = 4$ with squares. Note that the coincidences at even fillings correspond to a crossing of two levels with *antiparallel* spins. In Figs. 3 and 4(a), the coincidences at low, odd fillings (e.g., $\nu = 3$ and 5) are not as easy to see at low temperatures since the resistance minima remain strong as the two LLs, which have *parallel* spins, cross. Such behavior has been reported previously and has been interpreted as a signature of easy-plane ferromagnetism.[18–20] We note that our data taken at higher temperatures ($T = 0.31$ K) reveal a weakening of the $\nu = 5$ R_{xx} minimum at $\Delta = 35$ K, and of the $\nu = 3$ minimum at $\Delta = 58$ K;[21] these are marked by circles in Fig. 4(a). The crossings at higher odd fillings are clearly seen in Figs. 4(a) and 5; for example, the $\nu = 7$ R_{xx} minimum disappears at around $\Delta = 50$ K, and the $\nu = 9$ R_{xx} minimum around $\Delta = 40$ and 60 K.[22]

In Figs. 4(a) and 5 we include several solid white lines representing $\Delta = iE_C$, assuming GaAs band effective mass of $m^* = 0.067$ (in units of free electron mass). These lines indeed pass through the positions of the *observed* LL coincidences at odd-integer fillings, implying that Δ is not re-normalized at these coincidences. We will return to the possibility of the renormalization of Δ near coincidences later in the paper. The dashed lines in Figs. 4(a) and 5 represent $\Delta = iE_C \pm E_Z, i = 1,2, \ldots$, where g^* is chosen as a fitting parameter so that these lines pass through the *observed* coincidences at even-integer fillings. All the dashed lines in Figs. 4(a) and 5 are drawn using $g^* = 8.8$, except for the $\Delta = E_C - E_Z$ line, which is drawn using $g^* = 7.6$.

We conclude that g^* is enhanced by a factor of $\sim$20 relative to the GaAs band g factor (0.44). This enhancement is somewhat larger than the values reported for GaAs QWs with two subbands occupied. For example, Muraki *et al.*[19] reported a $\sim$tenfold enhancement of g^* for electrons in a 40-nm-wide QW with $n \sim 3 \times 10^{11}$ cm^{-2} while Zhang *et al.*[23] measured a $\sim$fivefold enhancement in a 24-nm-wide QW with $n \sim 7 \times 10^{11}$ cm^{-2}. In GaAs/AlGaAs heterojunction samples, Leadley *et al.*[24] report a density-dependent g^* which is about 14-fold enhanced at a density comparable to our sample density. It appears then that the enhancement depends on the QW width, confining potential, and electron density, and a systematic study of the enhancement would be an interesting future project. We would also like to emphasize that the dashed lines in Figs. 4(a) and 5 pass through nearly all of the observed coincidences quite well. Since each of these lines are drown using very similar g^*, the data imply that the enhancement is nearly independent of the filling factor. This is surprising, because an exchange-enhanced g^* is theoretically expected to depend on the filling factor.[25] We mention, however, that the observation of a significantly enhanced g factor which is essentially independent of the filling factor is not unprecedented and has been reported before for 2D electrons in GaAs[24] and in AlAs.[26,27]

We now focus on the main finding of our work, namely the correspondence between the stability of the FQH states and the position of E_F. Note in Figs. 3 and 4(a) that FQH states are observed only in certain ranges of Δ. For example, the $\nu = 10/3$ and $11/3$ states are seen in the regions marked by A and C in Fig. 4(a) but they are essentially absent in the B region. The $\nu = 13/3$ and $14/3$ states, on the other hand, are absent in regions D and F while they are clearly seen in regions E and G.

To understand this behavior, in the fan diagram of Fig. 4(b) we have highlighted the position of E_F as a function of Δ for different filling factors by color-coded lines. Concentrating on the range $3 < \nu < 4$ [green line in Fig. 4(b)], at small values of Δ (region A), E_F lies in the A0$\downarrow$ level. At higher Δ, past the first $\nu = 4$ coincidence which occurs when $\Delta = E_C - E_Z$, E_F is in the S1$\uparrow$ level (region B). Once Δ exceeds E_C, E_F lies in the A0$\uparrow$ level (region C) until the second $\nu = 4$ coincidence occurs when $\Delta = E_C + E_Z$. Note in Fig. 4(a) that strong FQH states at $\nu = 10/3$ and $11/3$ are seen in regions A and C. From the fan diagram of Fig. 4(b) it is clear that in these regions E_F is in the *ground-state* ($N = 0$) LLs of the asymmetric subband, that is, A0$\uparrow$ and A0$\downarrow$. In contrast, in region B, where the $10/3$ and $11/3$ states are essentially absent, E_F lies in an *excited* ($N = 1$) LL, namely, S1$\uparrow$. We conclude that the $10/3$ and $11/3$ FQH states are stable and strong when E_F lies in a ground-state LL.

The data in the range $4 < \nu < 5$ corroborate the above conclusion. In Fig. 4(b) we represent the position of E_F

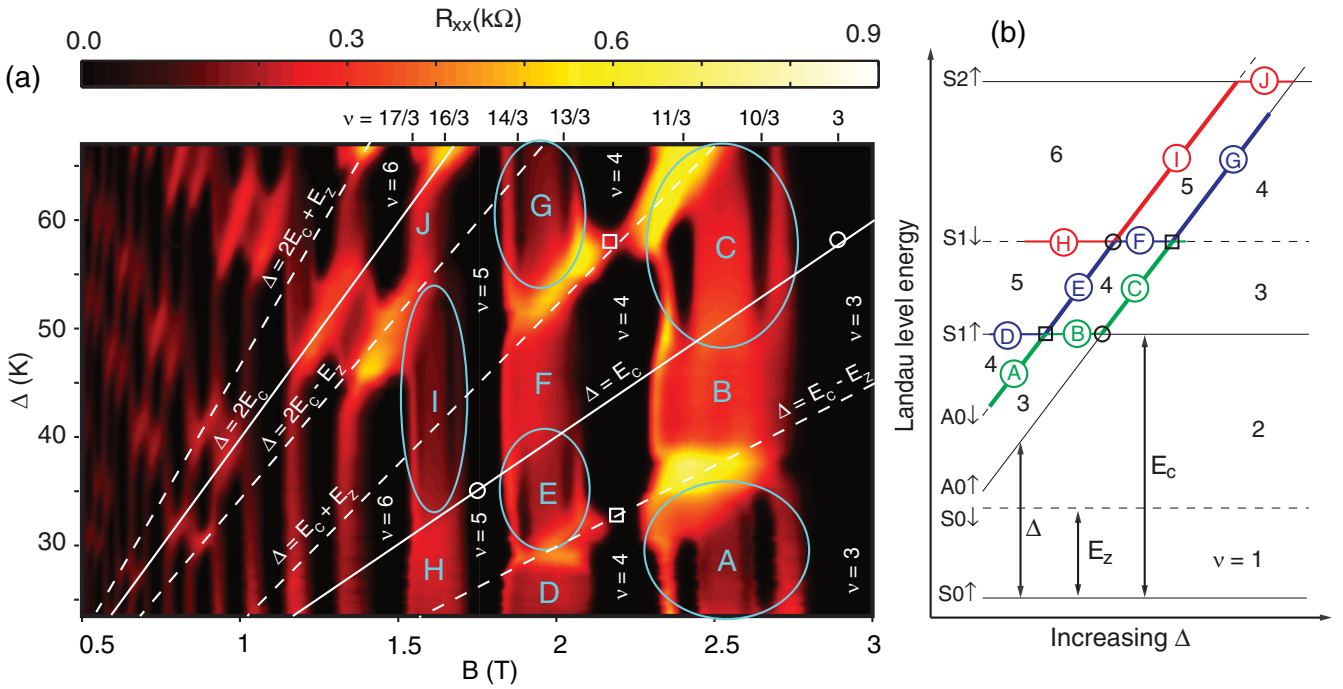

FIG. 4. (Color online) Evolution of R_{xx} data taken at a fixed density $n = 2.12 \times 10^{11}$ cm^{-2} as the subband separation (Δ) is increased. (a) A color-scale plot of the data shown in Fig. 3. The dark regions are where the integer or fractional quantum Hall states are observed at the indicated values of ν. The solid white lines denote $\Delta = E_C$ and $\Delta = 2E_C$, where E_C is the cyclotron energy. The dashed white lines are drawn such that they pass through the even-filling coincidences (see text). The cyan ellipses mark different regions (A, C, E, G, and I) where FQH states are seen. (b) Schematic electron Landau level diagram as a function of increasing Δ. The relevant energies Δ, the cyclotron energy (E_C), and the Zeeman energy (E_Z) are shown. The position of the Fermi level is plotted in different colors for several filling factor regions: $3 < \nu < 4$ (green), $4 < \nu < 5$ (blue), and $5 < \nu < 6$ (red). The letters correspond to the regions in the (a) panel; the regions where FQH states are observed are marked by thicker lines.

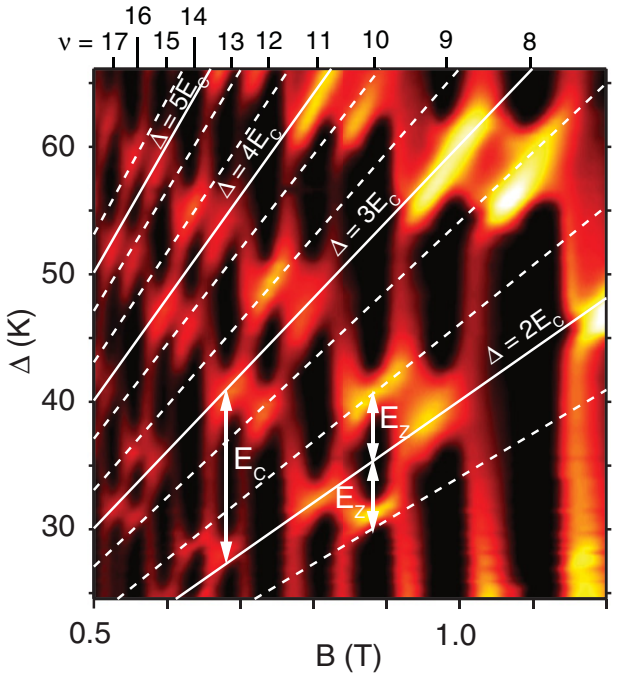

FIG. 5. (Color online) An expanded color-scale plot of R_{xx} data at low fields for $n = 2.12 \times 10^{11}$ cm^{-2}. The solid white lines denote $\Delta = iE_C$ for $i = 2, 3, 4, 5$. The dashed white lines represent $\Delta = iE_C \pm E_Z$, using a fixed $g^* = 8.8$ (see text).

in this filling range by a blue line. In regions E and G, E_F lies in the ground-state LLs of the asymmetric subband (A0↓ and A0↑), and these regions are indeed where the $\nu = 13/3$ and $14/3$ FQH states are seen. In regions D and F, on the other hand, E_F is in the excited LLs of the symmetric subband (S1↑ and S1↓), and the $13/3$ and $14/3$ FQH states are absent. Data at yet higher fillings ($5 < \nu < 6$) follow the same trend: FQH states at $\nu = 16/3$ and $17/3$ are seen in region I when E_F is in the A0↓ level,[28] but they are absent in regions H or J where E_F lies in the S1↓ or S2↑ levels.

In Fig. 6 we show additional data for a density of $n = 2.90 \times 10^{11}$ cm^{-2} in the same QW. Longitudinal and Hall resistance traces are shown in the bottom panels for three different values of Δ, and in each panel the calculated charge distribution (at $B = 0$) is also shown. In the top panels we show the positions of the LLs and E_F, corresponding to the filling factors in the bottom panels. In all cases, strong $q/3$ FQH states are observed when E_F lies in the A0↓ level. Note that the data shown in Fig. 6 are for asymmetric charge distributions. We would like to emphasize that strong $q/3$ states are also observed for symmetric (balanced) charge distributions; for example, see the bottom trace in Fig. 3, or the traces in Fig. 2(c) of Shabani *et al.*[14]

Next we address the FQH states observed at lower ν (<3) in our sample. Data are shown for $n = 2.12 \times 10^{11}$ cm^{-2} for the balanced QW ($\Delta = 24$ K) in Fig. 7; the R_{xx} trace

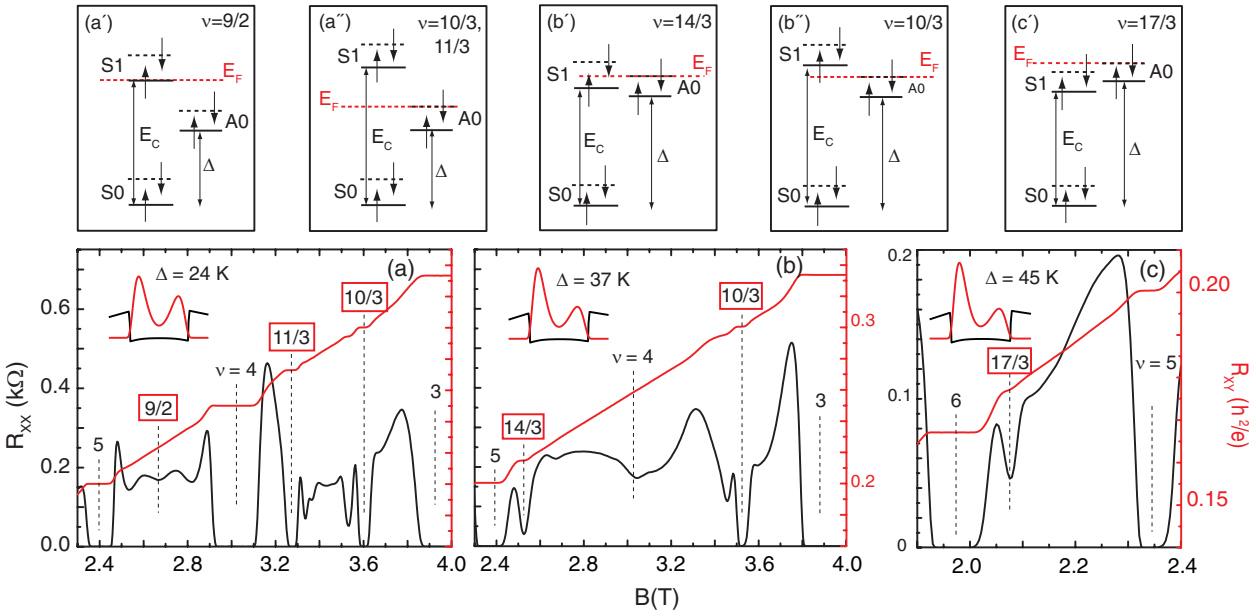

FIG. 6. (Color online) (a), (b), (c) Longitudinal (R_{xx}) and Hall (R_{xy}) resistances for the 55-nm-wide QW at a higher density $n = 2.90 \times 10^{11}$ cm^{-2}. Panels (a) and (b) share the same scales for R_{xx} and R_{xy}. The traces were taken at $T = 30$ mK, and the insets show the charge distributions calculated at $B = 0$. The LL diagrams for fractional fillings in panels (a), (b), and (c) are shown in (a′) and (a″), (b′) and (b″), and (c′), respectively. Fractional quantum Hall states at $\nu = 10/3$, $11/3$, $14/3$, and $17/3$ are clearly seen when E_F lies in either the A0↑ or A0↓ levels.

is an extension of the lowest trace shown in Fig. 3. In the range $1 < \nu < 3$, strong FQH states are seen at $\nu = 4/3$, $5/3$, $7/3$, and $8/3$. Data taken at yet higher magnetic fields (not shown) reveal the presence of a very strong FQH state at $\nu = 2/3$. From the fan diagram of Fig. 4(b), it is clear that E_F at these fillings lies in an $N = 0$ LL, namely, the A0↑ ($\nu = 7/3$ and $8/3$), S0↓ ($\nu = 4/3$ and $5/3$), or S0↑ ($\nu = 2/3$) levels.[29]

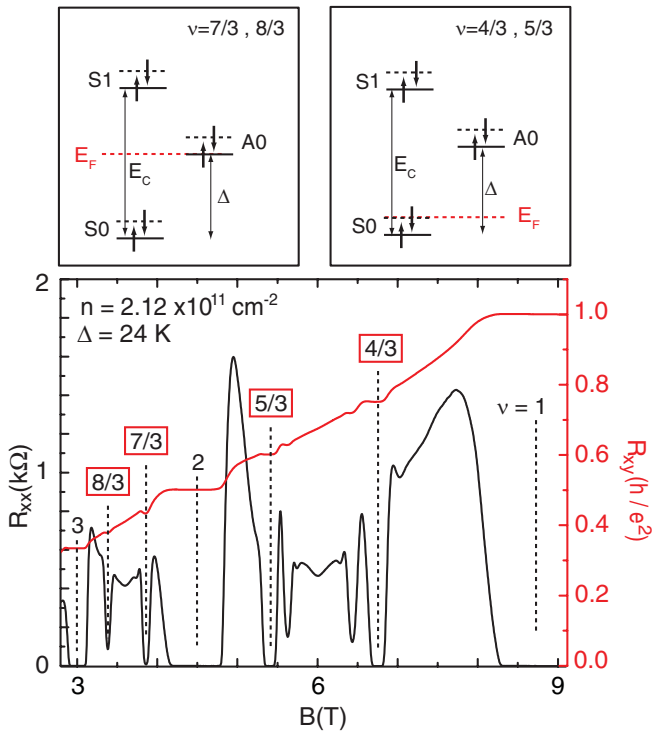

FIG. 7. (Color online) R_{xx} and R_{xy} traces at high magnetic fields and $T = 30$ mK for $n = 2.12 \times 10^{11}$ cm^{-2} for the balanced QW. Fractional quantum Hall states at $\nu = 4/3$, $5/3$, $7/3$, and $8/3$ are clearly seen. The upper panels show the LL diagrams and positions of E_F for the indicated fillings.

IV. DISCUSSION

Our observations provide direct evidence that the $q/3$ FQH states are strong when E_F resides in a ground-state ($N = 0$) LL, regardless of whether that LL belongs to the A or S subband. This finding implies that the node in the wave function in the *out-of-plane* direction does not significantly destabilize the $q/3$ FQH states. On the other hand, when E_F lies in an $N > 0$ LL, the wave function node(s) in the *in-plane* direction weaken or completely destabilize the $q/3$ FQH states. These conclusions are consistent with the data from single-subband samples,[4,6–8] as well as theoretical calculations.[5,9–13] In a composite Fermion picture, our data also imply that the fully occupied, lower-lying LLs are essentially inert and the composite Fermions are formed in the partially filled LL where E_F lies. The composite Fermions, however, could have a spin and/or subband degree of freedom, as we discuss at the end of this section (see also Ref. 14).

Our data also allow us to assess the stability of the FQH states as two LLs approach each other. It is clear in Fig. 4(a) that R_{xx} data near LL coincidences at even ($\nu = 4$ and 6) or odd ($\nu = 3$ and 5) fillings exhibit different features. As we approach the $\Delta = E_C - E_Z$ line from the A region, the $10/3$ and $11/3$ FQH states remain strong and abruptly disappear before they reach the dashed line, near which no FQH states but rather large R_{xx} peaks are seen. A similar statement can be made regarding the stability of the other $q/3$ FQH states when

a dashed line is approached from a circled region. All these cases correspond to the crossing of two LLs with *antiparallel* spins. Near the coincidences where two *parallel* spin LLs are crossing at E_F, on the other hand, instead of abruptly disappearing and being replaced by R_{xx} peaks, the $q/3$ states persist and gradually become weaker. For example, the $\nu = 10/3$ FQH state persists very close to the $\Delta = E_C$ line as we approach this line from region C. These observations suggest that the relative spins of the two approaching LLs play a role in the stability of the $q/3$ FQH states.

It is worth reiterating that, as is evident from Figs. 3 and 4(a) data, the relative spins of the two approaching LLs also play a crucial role in the stability of the *integer* quantum Hall (IQH) states. For antiparallel-spin LLs, the IQH state (e.g., at $\nu = 4$) becomes very weak or completely disappears, while for the parallel-spin LLs the IQH state (e.g., at $\nu = 3$), remains strong. This behavior has been attributed to easy-axis (for an antiparallel-spin crossing) and easy-plane (for a parallel-spin crossing) ferromagnetism.[18–20]

In order to further discuss the stability of the FQH states near LL crossings, we examine the possibility that Δ is renormalized near LL coincidences. As pointed out in Ref. 30, when only a small number of quantized LLs belonging to two different subbands are occupied, the distribution of electrons between these levels does not necessarily match the $B = 0$ subband densities. This leads to a mismatch between the total electron charge density distributions at $B = 0$ and high B. A pinning of two crossing LLs belonging to different electric subbands and a charge transfer between these levels can help bring these distributions closer to each other. The pinning also implies that the subband separation in magnetic field [$\Delta(B)$] is renormalized and is different from the zero-field subband separation (Δ).[30–32] To examine the role of such a pinning quantitatively, we performed self-consistent calculations of the potential energy and charge distribution at high B, similar to those described in Ref. 29. The calculations provide the boundaries inside which two LLs are pinned together at E_F.

Examples of the calculated boundaries are shown by solid lines (rhombohedral-shaped "boxes") in Fig. 8(a). Each box marks the boundary inside which the two crossing LLs (at E_F) are pinned together near an integer filling. To explain how we calculated these boundaries, let us focus on the lower left box labeled $\Delta(B) = E_C$ in Fig. 8(a); we will refer to this box as the $\nu = 5$ box. Inside this box, which corresponds to the crossing of the A0↓ and S1↓ levels near $\nu = 5$, the *in-field* subband separation is given by $\Delta(B) = E_C$. This expression ensures that $\Delta(B)$ is fixed at a given B, consistent with the pinning of the S1↓ and A0↓ levels. Consider next a series of in-field self-consistent calculations, all done for a total density equal to 2.12×10^{11} cm^{-2} but each corresponding to a different QW asymmetry. For each QW asymmetry, the in-field charge distribution is given by

$$\rho(B) = e(eB/h)[\nu_S \cdot |\psi_S(B)|^2 + \nu_A \cdot |\psi_A(B)|^2]. \quad (1)$$

Now, for each point on the $\nu = 5$ box boundary, ν_S and ν_A have specific and well-defined values. For example, at $\nu = 5$ ($B = 1.75$ T), for which we show the results of our self-consistent calculations in Figs. 8(b)–8(d), we have $\nu_S = 4$ and $\nu_A = 1$ for the upper boundary and $\nu_S = 3$ and $\nu_A = 2$ for the lower one. Note that $\nu_S = 4$ and $\nu_A = 1$ at the upper boundary corresponds to level A0↓ having just depinned from S1↓ and moved above it [Fig. 8(b)], while $\nu_S = 3$ and $\nu_A = 2$ corresponds to A0↓ having just moved below S1↓ [Fig. 8(d)]. Focusing on the upper boundary at $\nu = 5$, we set $\nu_S = 4$ and $\nu_A = 1$ in Eq. (1), and perform a series of self-consistent calculations, each for a different QW symmetry. One of these calculations in particular has a subband separation which is equal to $\Delta(B) = E_C$ (=35 K for $B = 1.75$ T). This particular

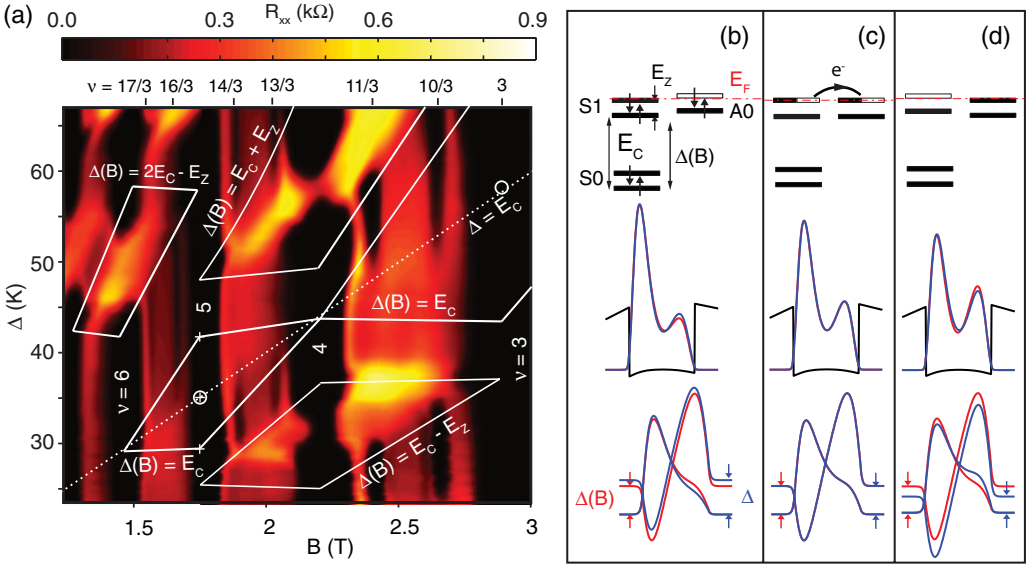

FIG. 8. (Color online) (a) Color-scale plot of R_{xx} data is shown again for $n = 2.12 \times 10^{11}$ cm^{-2}. The rhombohedral boxes show the calculated boundaries within which the crossing LLs are pinned together at E_F. (b)–(d) Schematic LL diagrams (top), charge distributions (middle), and wave functions (bottom), self-consistently calculated at $B = 0$ (blue) and at $\nu = 5$ (red). In (b)–(d), the filling factor of the S1↓ level equals 1, 0.5, and 0, respectively. In each panel, the calculated wave functions are shifted vertically according to the values of Δ and $\Delta(B)$.

QW asymmetry gives the upper boundary at $B = 1.75$ T. We then calculate the zero-field subband separation for this QW asymmetry, which turns out to be $\Delta = 42$ K, and mark it in Fig. 8(a) as the upper boundary for the pinning of the A0↓ and S1↓ levels at $B = 1.75$ T. Note that the above procedure ensures that, at the upper boundary, $\Delta(B)$ at $B = 1.75$ T is equal to 35 K and the electron charge distributions at zero field and at 1.75 T are very close to each other [see the blue and red curves in Fig. 8(b)]. For the lower boundary of the $\nu = 5$ box at $B = 1.75$ T, we follow the same procedure but use $\nu_S = 3$ and $\nu_A = 2$ in the calculations. We find that the QW asymmetry that gives $\Delta(B) = 35$ K corresponds to a zero-field Δ of 29 K which we mark in Fig. 8(a) as the lower boundary at 1.75 T.

The rest of the $\nu = 5$ box boundaries in Fig. 8(a) are determined in a similar fashion. For example, at a field of 2.00 T [$\nu = 4.38$, $\Delta(B) = 40$ K], to determine the upper boundary we set $\nu_S = 4$ and $\nu_A = \nu - \nu_S = 0.38$ and do a series of in-field self-consistent calculations to find the QW asymmetry that gives a subband separation of 40 K. We then calculate the zero-field subband separation for this particular QW asymmetry; this turns out to be 25 K which we mark as the upper boundary of the $\nu = 5$ box at $B = 2.00$ T. Following the same procedure, we also find and draw the boundaries for the pinning of the S1↑ and A1↑ LLs when they coincide (at E_F) at and near $\nu = 3$. These boundaries are shown in Fig. 8(a) by the upper right box labeled $\Delta(B) = E_C$. Similarly, we calculated the boundaries for the pinning of coinciding LLs near $\nu = 4$ and 6, and show these in Fig. 8(a). For the box labeled $\Delta(B) = 2E_C - E_Z$ we assumed $g^* = 8.8$, while for the two boxes labeled $\Delta(B) = E_C \pm E_Z$ we used $g^* = 7.6$. We note that the boundaries of these boxes depend weakly on the value of g^* used. For example, the lower boundary of the $\Delta(B) = E_C - E_Z$ box centered around $\nu = 4$ moves up/down by ∼0.6 K, and the upper boundary by ∼3 K, if we use a g^* which is smaller/larger than 7.6 by 3 (i.e., if we use $g^* = 4.6$ or 10.6).

Despite the simplicity of our simulations, the calculated boundaries for the LL crossings near $\nu = 4$ appear to match the observed features of the data reasonably well. For example, in Fig. 8(a) as we approach the lower right boundaries of the $\Delta(B) = E_C \pm E_Z$ boxes from below [i.e., from regions A or C in Fig. 4(a)], the $\nu = 10/3$ and $11/3$ FQH states abruptly disappear when the A0↓ level reaches the S1↑ or S1↓ level at these boundaries. A similar statement can be made regarding the FQH states at $\nu = 13/3$ and $14/3$: these states disappear near the upper left boundary of the $\Delta(B) = E_C \pm E_Z$ boxes.[33] We note that in Fig. 8(a) the $\nu = 10/3$ and $11/3$ fractional states appear to slightly penetrate inside the $\Delta(B) = E_C \pm E_Z$ boxes. This is likely because of the inadequacies and uncertainties in our calculations. We emphasize that our simulations, which are based on solving Poisson and Schroedinger equations self-consistently, ignore the exchange-correlation effects and use a constant g factor for an entire box. It is possible that calculations which treat many-body interactions properly would account for the ∼2–3 K discrepancy between the boundaries of the boxes and the regions where the FQH states are experimentally observed.

The situation appears to be different, however, as the boundaries of the $\Delta(B) = E_C$ boxes centered at odd fillings are approached. The $q/3$ fractional states do not disappear near these boundaries; instead they seem to penetrate deep inside these boxes and disappear slowly when the $\Delta(B) = E_C$ line [the dotted line in Fig. 8(a)] is reached.[34] This is clearest in Fig. 8(a) for the $\nu = 10/3$ and $14/3$ fractional states. Given that the calculations involve only the cyclotron energy and not the Zeeman energy, we do not believe that it is the inaccuracy of the calculation which leads to this surprising observation.

Note that a main difference between the boxes centered at odd compared to even fillings is that an odd-filling box corresponds to the crossing of two LLs with parallel spins, while the two LLs crossing inside an even-filling box have antiparallel spins. We believe that the observations described in the preceding two paragraphs might be explained in terms of easy-axis vs easy-plane ferromagnetism to which we alluded before.[18–20] The sudden disappearance of FQH states when two LLs with antiparallel spins become degenerate at E_F is consistent with easy-axis ferromagnetism. Electrons in these levels could condense into domains with opposite magnetization. The large resistance [bright colors in Figs. 4(a) and 8(a)] can be attributed to electron scattering and enhanced dissipation at these domain walls.[35,36] When the two approaching LLs have parallel spins, on the other hand, we expect the system to exhibit easy-plane anisotropy. Instead of forming ferromagnetic domains, the wave functions of the electrons in these levels can mix and fractional states are seen deep inside a LL crossing box. These states gradually weaken and eventually disappear as their wave function progressively assumes the character of the $N = 1$ LL wave function.

We highlight three further observations. First, strong FQH states at large $q/3$ fillings have been recently observed in very high quality graphene samples.[37] These states qualitatively resemble what we see in our two-subband system. It is tempting to associate the valley degree of freedom in graphene with the subband degree of freedom in our sample. But the LL structure in graphene is of course different from GaAs so it is not obvious if this association is valid. Second, data taken in the $N = 1$ LL at very low temperatures and in the highest quality, single-subband samples exhibit FQH states at even-denominator fillings $\nu = 5/2$ and $7/2$.[38,39] In the traces shown in Fig. 3, we do not see any even-denominator states when $N = 1$, for example, at $\nu = 7/2$ in region B where E_F is in the S1↑ level. However, in the same sample, at higher densities ($n > 3.4 \times 10^{11}$ cm^{-2}) and at low temperatures ($T = 30$ mK), we do indeed observe a FQH state at $\nu = 7/2$ flanked by very weak $10/3$ and $11/3$ states when E_F lies in the S1↑ level.[14]

Third, in the $N = 0$ LL, high-quality samples show strong higher-order, odd-denominator FQH states at composite Fermion filling factor sequences such as 2/5, 3/7, 4/9, etc.[3] We do observe a qualitatively similar behavior in our data when E_F is in an $N = 0$ LL. For example, in region A [Figs. 3 and 4(a)] we see weak but clear minima at $\nu = 17/5$ next to the $10/3$ minimum. Again, at higher densities and low temperatures, such states become more developed.[14] In Fig. 1(b), for example, there are strong minima at $\nu = 12/5$ and $13/5$, adjacent to the $7/3$ and $8/3$ minima, and at $17/5$ and $18/5$, adjacent to the $10/3$ and $11/3$ minima. These states, as well as the $q/3$ states, exhibit subtle evolutions

even when E_F lies within a fixed $N = 0$ LL, consistent with the presence of composite Fermions which have spin and/or subband degrees of freedom.[14] A related question concerns the role of charge distribution symmetry in the stability of the $q/3$ states. In other words, in a QW with fixed width, density, and filling, and with E_F in a particular $N = 0$ LL, how does the strength of given a FQH state at a particular filling vary with charge distribution symmetry. We do not have data to answer this question quantitatively, but the data we present here clearly indicates that a primary factor determining the strength of the $q/3$ FQH states is whether or not E_F lies in an $N = 0$ LL.

V. SUMMARY

In conclusion, the position of E_F is what determines the stability of odd-denominator, $q/3$ FQH states at a given filling factor. When E_F lies in a ground-state ($N = 0$) LL, the $q/3$ FQH states are stable and strong, regardless of whether that LL belongs to the symmetric or antisymmetric subband. This observation implies that the wave function node in the out-of-plane direction is not detrimental to the stability of these FQH states. Also, the stability of the $q/3$ FQH states near the crossing of two LLs depends on the relative spin polarization of these levels.

ACKNOWLEDGMENTS

We acknowledge support through the NSF (DMR-0904117 and MRSEC DMR-0819860) for sample fabrication and characterization, and the DOE BES (DE-FG0200-ER45841) for measurements. We thank J. K. Jain and Z. Papic for illuminating discussions.

[1] D. C. Tsui, H. L. Stormer, and A. C. Gossard, Phys. Rev. Lett. **48**, 1559 (1982).
[2] R. B. Laughlin, Phys. Rev. Lett. **50**, 1395 (1983).
[3] J. K. Jain, *Composite Fermions* (Cambridge University Press, New York, 2007).
[4] W. Pan, J.-S. Xia, V. Shvarts, D. E. Adams, H. L. Stormer, D. C. Tsui, L. N. Pfeiffer, K. W. Baldwin, and K. W. West, Phys. Rev. Lett. **83**, 3530 (1999).
[5] C. Töke, M. R. Peterson, G. S. Jeon, and J. K. Jain, Phys. Rev. B **72**, 125315 (2005).
[6] M. P. Lilly, K. B. Cooper, J. P. Eisenstein, L. N. Pfeiffer, and K. W. West, Phys. Rev. Lett. **82**, 394 (1999).
[7] R. Du, D. Tsui, H. Stormer, L. Pfeiffer, K. Baldwin, and K. West, Solid State Commun. **109**, 389 (1999).
[8] G. Gervais, L. W. Engel, H. L. Stormer, D. C. Tsui, K. W. Baldwin, K. W. West, and L. N. Pfeiffer, Phys. Rev. Lett. **93**, 266804 (2004).
[9] F. D. M. Haldane, in *The Quantum Hall Effect*, edited by R. E. Prange and S. M. Girvin (Springer, New York, 1987), pp. 303–352.
[10] A. H. MacDonald and S. M. Girvin, Phys. Rev. B **33**, 4009 (1986).
[11] N. d'Ambrumenil and A. Reynolds, J. Phys. C **21**, 119 (1988).
[12] A. A. Koulakov, M. M. Fogler, and B. I. Shklovskii, Phys. Rev. Lett. **76**, 499 (1996).
[13] R. Moessner and J. T. Chalker, Phys. Rev. B **54**, 5006 (1996).
[14] J. Shabani, Y. Liu, and M. Shayegan, Phys. Rev. Lett. **105**, 246805 (2010).
[15] Our sample is the same as the one used in Ref. 14. Based on our careful measurements of the subband separation (Δ) while imbalancing the QW (see Fig. 2), we conclude that the QW has a width of 55 nm, slightly smaller than 56 nm which was quoted in Ref. 14. We emphasize that throughout our paper we use the experimentally measured values of Δ, and that the exact width of the QW has no bearing on our conclusions.
[16] Y. W. Suen, H. C. Manoharan, X. Ying, M. B. Santos, and M. Shayegan, Phys. Rev. Lett. **72**, 3405 (1994).
[17] J. Shabani, T. Gokmen, Y. T. Chiu, and M. Shayegan, Phys. Rev. Lett. **103**, 256802 (2009).
[18] T. Jungwirth, S. P. Shukla, L. Smrcka, M. Shayegan, and A. H. MacDonald, Phys. Rev. Lett. **81**, 2328 (1998).
[19] K. Muraki, T. Saku, and Y. Hirayama, Phys. Rev. Lett. **87**, 196801 (2001).
[20] K. Vakili, T. Gokmen, O. Gunawan, Y. P. Shkolnikov, E. P. De Poortere, and M. Shayegan, Phys. Rev. Lett. **97**, 116803 (2006).
[21] J. Shabani, Ph.D. thesis, Princeton University, 2011.
[22] We note that when the charge distribution is nearly symmetric, LL coincidences at even fillings are also difficult to see at very low temperatures. For example, there is a coincidence at $\nu = 8$ at $\Delta \simeq 26$ K but we can only see a weakening of the R_{xx} minimum at $T \gtrsim 0.3$ K.
[23] X. C. Zhang, I. Martin, and H. W. Jiang, Phys. Rev. B **74**, 073301 (2006).
[24] D. R. Leadley, R. J. Nicholas, J. J. Harris, and C. T. Foxon, Phys. Rev. B **58**, 13036 (1998).
[25] T. Ando and Y. Uemura, J. Phys. Soc. Jpn. **37**, 1044 (1974).
[26] S. J. Papadakis, E. P. De Poortere, and M. Shayegan, Phys. Rev. B **59**, R12743 (1999).
[27] Y. P. Shkolnikov, E. P. De Poortere, E. Tutuc, and M. Shayegan, Phys. Rev. Lett. **89**, 226805 (2002).
[28] The $E_C + E_Z$ line going through region I does not correspond to a LL coincidence at the Fermi energy in this region; this should be evident from Fig. 4(b) diagram. The same is true about the $2E_C - E_Z$ line as it goes through region G.
[29] Traces taken at higher values of Δ reveal that the $\nu = 7/3$ and $8/3$ states remain strong up to the $\nu = 3$ coincidence. Past this coincidence, the $7/3$ and $8/3$ states become weaker, consistent with the fact that E_F now lies in an excited LL [the S1↑ level, see Fig. 4(b)].
[30] S. Trott, G. Paasch, G. Gobsch, and M. Trott, Phys. Rev. B **39**, 10232 (1989).
[31] A. G. Davies, C. H. W. Barnes, K. R. Zolleis, J. T. Nicholls, M. Y. Simmons, and D. A. Ritchie, Phys. Rev. B **54**, R17331 (1996).
[32] V. V. Solovyev, S. Schmult, W. Dietsche, and I. V. Kukushkin, Phys. Rev. B **80**, 241310 (2009).
[33] Similarly, the $\nu = 16/3$ and $17/3$ FQH states disappear at the lower right boundary of the $\Delta(B) = 2E_C - E_Z$ box.
[34] In fact, in very high quality samples and at very low temperatures, the $q/3$ FQH states exist on both side of the $\Delta = E_C$ line and do not disappear as this line is crossed. For example, the $\nu = 7/3$ FQH state is stable (but weak) when E_F is in the S1↑ level

and becomes monotonically stronger as the S1↑ and A0↑ levels cross and E_F moves to the A0↑ level (Y. Liu, D. Kamburov, M. Shayegan, L. N. Pfeiffer, K. W. West, and K. W. Baldwin, e-print arXiv:1106.0089v2).

[35]E. P. De Poortere, E. Tutuc, S. J. Papadakis, and M. Shayegan, Science **290**, 1546 (2000).

[36]T. Jungwirth and A. H. MacDonald, Phys. Rev. Lett. **87**, 216801 (2001).

[37]C. R. Dean, A. F. Young, P. Cadden-Zimansky, L. Wang, H. Ren, K. Watanabe, T. Taniguchi, P. Kim, J. Hone, and K. L. Shepard, Nature Phys. **7**, 693 (2011).

[38]R. Willett, J. P. Eisenstein, H. L. Störmer, D. C. Tsui, A. C. Gossard, and J. H. English, Phys. Rev. Lett. **59**, 1776 (1987).

[39]W. Pan, J. S. Xia, H. L. Stormer, D. C. Tsui, C. Vicente, E. D. Adams, N. S. Sullivan, L. N. Pfeiffer, K. W. Baldwin, and K. W. West, Phys. Rev. B **77**, 075307 (2008).